International Journal of Plasticity 27 (2011) 920–939

Contents lists available at ScienceDirect

International Journal of Plasticity

journal homepage: www.elsevier.com/locate/ijplas

Effects of the strain-hardening exponent on two-parameter characterizations of surface-cracks under large-scale yielding

Shawn A. English, Nagaraj K. Arakere *

Department of Mechanical and Aerospace Engineering, University of Florida, Gainesville, FL 32611-6300, USA

ARTICLE INFO

Article history:
Received 29 June 2010
Received in final revised form 9 September 2010
Available online 30 October 2010

Keywords:
Surface cracks
Constraint effects
Finite element analysis
Large-scale yielding
Ductile fracture

ABSTRACT

The influence of strain hardening exponent on two-parameter J–Q near tip opening stress field characterization with modified boundary layer formulation and the corresponding validity limits are explored in detail. Finite element simulations of surface cracked plates under uniaxial tension are implemented for loads exceeding net-section yield. The results from this study provide numerical methodology for limit analysis and demonstrate the strong material dependencies of fracture parameterization under large scale yielding. Sufficient strain hardening is shown to be necessary to maintain J–Q predicted fields when plastic flow progresses through the remaining ligament. Lower strain hardening amplifies constraint loss due to stress redistribution in the plastic zone and increases the ratio of tip deformation to J. The onset of plastic collapse is marked by shape change and/or rapid relaxation of tip fields compared to those predicted by MBL solutions and thus defining the limits of J–Q dominance. A radially independent Q-parameter cannot be evaluated for the low strain hardening material at larger deformations within a range where both cleavage and ductile fracture mechanisms are present. The geometric deformation limit of near tip stress field characterization is shown to be directly proportional to the level of stress the material is capable of carrying within the plastic zone. Accounting for the strain hardening of a material provides a more adjusted and less conservative limit methodology compared to those generalized by the yield strength alone. Results from this study are of relevance to establishing testing standards for surface cracked tensile geometries.

1. Introduction

Plastic deformation precedes fracture in metals and their alloys and resistance to fracture is therefore directly related to the development of the plastic zone at the crack tip. Among the major causes of metallic structural failure is the nucleation and propagation of cracks from regions of high stress concentration such as notches and surface flaws, due to both monotonic and fatigue loading. Understanding the evolution of plasticity in notches and cracks is therefore important for predicting fracture behavior of critical load bearing structures in many engineering applications. Consequently, development of crack tip elastic–plastic fields, as a function of load configuration, geometry, monotonic and cyclic strain hardening behavior, and constraint effects have been subject of intensive study.

Behavior of the crack tip in the plastic zone for strain hardening materials under small-scale yielding for symmetric (Mode I) or antisymmetric (Mode II) two-dimensional (2D) stress distribution has been presented in the widely referenced HRR articles by Hutchinson (1968a, b) and Rice and Rosengren (1968). Extensions to combinations of Mode I and Mode II loadings were presented by Shih (1973, 1974). Comprehensive literature reviews of plane-strain fracture mechanics and

* Corresponding author. Tel.: +1 352 392 0856; fax: +1 352 392 1071.
E-mail address: nagaraj@ufl.edu (N.K. Arakere).

0749-6419/$ - see front matter © 2010 Elsevier Ltd. All rights reserved.
doi:10.1016/j.ijplas.2010.10.002

Nomenclature

t	thickness
L	half length
l	general characteristic length
w	half width
a	crack depth
c	half crack width
r	radial distance from crack tip
J	J-integral
T	T-stress
Q	near crack stress difference parameter
σ_o	reference yield stress
ε_o	yield strain
n	strain hardening exponent for a linear plus power law material
σ_∞	far-field stress in the loading direction
σ_{Net}	average stress in the opening direction over the remaining area in the crack plane
δ	far-field displacement
u_y	crack tip blunting displacement
θ	angle in plane perpendicular to crack front, $\theta = 0^\circ$ is in the growth direction
ϕ	angle measured along the crack front in the crack plane

crack tip field characterization are found in Anderson (2004), Irwin and Paris (1971), McClintock (1971), Panayotounakos and Markakis (1991), Rice and Rosengren (1968).

The aforementioned papers refer to fracture prediction using single parameter (K for brittle fracture and J for ductile fracture) crack tip field characterizations. The J-integral alone does not uniquely and accurately describe the crack tip fields and resistance against initiation of ductile crack growth when constraint effects arising from geometry and load configuration are considered. The constraint can be thought of as a structural obstacle against plastic deformation induced mainly by the geometrical and physical boundary conditions (Yuan and Brocks, 1991). Constraint effects can also arise from mismatch of material properties in a heterogeneous joint (English et al., 2010). Under these conditions, a second parameter, in addition to the J or K, is introduced to quantify the crack tip constraint. Crack tip triaxiality, which is defined as the ratio of hydrostatic pressure to von Mises stress, or a parameter that maintains a linear relationship with triaxiality, can be used as a constraint parameter for predicting ductile crack growth. The in-plane constraint is influenced by the specimen dimension in the direction of crack growth or the length of the uncracked ligament, and by global load configuration (bending or tension), whereas the out-of-plane constraint is controlled by the specimen dimension parallel to the crack front or the specimen thickness, for thorough-thickness cracks (Giner et al., 2010). Out-of-plane constraint is typically denoted as a plane-strain (high triaxiality) or plane-stress (low triaxiality) state. In finite thickness fracture geometries, where the points are embedded entirely in material, there exists a state of plane-strain near the crack tip, the exception being very thin films (O'Dowd, 1995; Shih and O'Dowd, 1993; Wang, 2009).

1.1. J-T and J–Q characterization of near tip fields

Williams (1957) showed the existence of a non-singular in-plane normal stress component (T-stress) for linear elastic material. The significance of the T-stress on the size and shape of the plastic zone under small-scale yielding (SSY) conditions was shown by Larsson and Carlsson (1973), Rice (1974), O'Dowd and Shih (1991, 1992), Sharma and Aravas (1991) show the important role played by higher order terms in asymptotic solutions of crack tip fields and demonstrate that a two-parameter characterization of the crack tip fields involving J and a triaxiality or constraint parameter Q is necessary to satisfactorily describe the configuration dependence of fracture response of isotropic plastic solids, particularly under large scale yielding conditions. The use of a single parameter characterization (K or J) is limited to geometries that maintain a high constraint, such as the compact tension (C(T)) specimen, where the in-plane stresses are dominated by bending. The Q stress difference factor has been found to maintain a material dependent linear relationship with near tip triaxiality independent of geometry, dimensions and deformation level. Moreover, the Q factor is shown to accurately predict near tip stress and strain fields, particularly plastic strains, and therefore can be used as a ductile fracture parameter (Henry and Luxmoore, 1997; Kikuchi, 1995).

A significant body of work has focused on two-parameter characterization of through-thickness cracks while limited work has been done on surface crack geometries. Wang (1993) established the two-parameter characterization with modified boundary layer (MBL) reference solutions to topographical planes perpendicular to the crack front in surface crack tension (SC(T)) and surface crack bend (SC(B)) geometries. Wang (2009) investigated Q as a function of load and radial distance from the crack tip for surface crack uniaxial and biaxial tension models.

A J–Q family of fields generated with MBL formulation is used as a comparison for assessing near tip J–Q dominance in actual structures. A near tip region is said to have J–Q dominance if the stress and strain distributions match the MBL reference field when the length scale is normalized by J/σ_o, where σ_o is the yield stress. Shih et al. (1993), O'Dowd (1995) in addressing the limitations of plane-strain references applied to three-dimensional geometries, suggested that as the distance from the crack tip becomes small, the out of plane (parallel to the crack front) strains become negligible when compared to the in-plane singular fields. Therefore, plane-strain MBL prediction of surface crack front stress fields should be accurate as the distance from the crack tip approaches zero.

1.2. Fracture prediction

Two-parameter fracture mechanics is important in engineering applications because it provides a more adjusted assessment of failure limits (Cicero et al., 2010; Silva et al., 2006). The primary source of enhancement stems from the constraint effects on near tip plastic deformations and subsequent effect on critical loads. Iwamoto and Tsuta (2002), Li and Chandra (2003), in their studies of crack growth characteristics in ductile materials, describe the direct influence of plastic strain and strain-induced material transformations at the crack tip on apparent fracture toughness. Faleskog (1995) showed experimentally how an increase in the constraint factor Q results in a decrease in the critical value of J. (Chao and Zhu (2000), MacLennan and Hancock (1995)) numerically and experimentally verified this effect on J-resistance (J–R) curves and failure assessment diagrams (FAD), respectively, with the highest constraint geometries having the lowest resistance. Similar results can be found throughout literature and it is now generally accepted that the increase in energy dissipation through plastic deformation due to loss of constraint can account for the increase in apparent fracture toughness.

1.3. Deformation limits

Many investigators have examined single and two-parameter characterizations limits (Kim et al., 2003; Larsson and Carlsson, 1973; McMeeking and Parks, 1979; O'Dowd and Shih, 1991, 1992; O'Dowd, 1995; Varias and Shih, 1993; Wang, 1993; Wang and Parks, 1995; Wang, 2009; Zhu and Chao, 2000). In single parameter fracture mechanics, the dominance limit of the asymptotic term is controlled by geometry and load/deformation. With the introduction of a non-singular geometry dependent constraint term, such as T or Q, the limits of characterization can be expressed by a load or deformation term. Wang and Parks (1995) considered the parametric limits of the constraint corrected asymptotically singular near tip stress fields based on crack tip deformations measured by J/σ_o relative to a characteristic length l, such as the remaining ligament or crack depth. The limiting relative local deformation factor $l\sigma_o/J_{cr}$, where J_{cr} is the J-integral at which two-parameter dominance of near tip fields cannot be assured, has been suggested by many investigators and is a requirement in ASTM E1820 for compact tension (C(T)) and single edge notched bend (SEN(B)) specimens (ASTM, 2006). This factor is dependent on loading conditions and material parameters, but given a proper definition of l and methodology to determine field dominance, a conservative limit locus can be found.

Geometries with deformation limit loads below critical fracture load will often have inflated toughness values with increased scatter. However, stress fields predicted using a micromechanical model within two-parameter deformation limits can be used to construct a constraint modified locus for cleavage fracture (Faleskog, 1995). In addition to experimentally establishing J and Q as accurate predictors of cleavage fracture in surface crack tensile (SC(T)) specimens, Faleskog (1995) provides a reasonable verification for the J–Q approach. He observes that the hoop stress ($\sigma_{\theta\theta}$) deviator of the Q defined difference fields is relatively consistent along the crack front for loads causing cleavage fracture, providing verification that Q is a proper measure of triaxiality. In addition, he uses MBL predicted opening stress fields to prove the existence of J–Q dominance in the crack plane at the cleavage fracture initiation positions along the crack front. The preliminary limitations analysis by MacLennan and Hancock (1995) of opening stress fields compared to MBL predictions is used to validate their experimentally constructed modified FAD approach.

To achieve a proper verification of the J–Q deformation limits, micro-scale deformation data and detailed near tip stresses are necessary. Therefore, finite element analysis is used to extrapolate experimental data in order to verify the existence of J–Q fields, as in MacLennan and Hancock (1995). Furthermore, the loss of two-parameter near tip field dominance can only be predicted using numerical methods and can be observed secondarily from various experimental results.

Paul and Khan (1998) in studying finite element models of a centrally cracked thin circular disk show that the inability to maintain hydrostatic pressure accounts for the reduced stress state at the crack front even with small strain approximations, but uncontained hydrostatic pressure very close to the crack tip results in high triaxiality and a maximum opening stress hump. This region, denoted as the process zone, is where damage from void coalescence and crack growth commonly takes place (Xia and Shih, 1995). This phenomenon can help to explain the near tip stress field variances from MBL predicted stresses, namely the rapid opening stress reduction at distances after the hump for large levels of deformation. The importance of including effects of hydrostatic stress and the third invariant of the stress deviator on stress state computation has been shown by Bai and Wierzbicki (2008), Gao et al. (2009, 2010) since it can play an important role on both the plastic response and ductile fracture behavior of certain aluminum alloys.

Ductile fracture analysis can be used subsequent to or in conjunction with traditional fracture parameterizations and has been the topic of much interest (Li et al., 2010; Mirone and Corallo, 2010; Wei and Xu, 2005; Xue et al., 2010). Li et al. (2010) give a thorough analysis of ductile fracture computational techniques and experimental results for a power-law material in

which the undamaged response follows J_2 plasticity theory. Although this initial isotropic material model is widely used for numerical evaluation of fracture parameters and near tip stress field analysis, ductile fracture techniques using void growth, shear band and anisotropy are necessary for accurate prediction of critical failure beyond limit deformations (Huespe et al., 2009; Sun et al., 2009). These types of analyses are important for the failure assessment of structures undergoing plastic deformations during normal operation in which the combination of geometry and plastic material properties prevents single and two-parameter fracture prediction but add a greater level of complexity.

1.4. Strain hardening effects on surface crack deformation limits

Surface cracks are among the most common flaws present in structural components and frequently the most critical in terms of limiting structural life, for both ductile and brittle materials (Evans and Riley, 1983; Leach et al., 2007). The geometry and loading conditions of surface cracks in actual structures will often be more complex than in laboratory specimens. Specifically, the near tip constraint conditions of a surface crack for both specimens and structures must be accounted for in order to compare accurately the failure conditions. Without a two-dimensional failure locus predicting values of the critical crack driving force as a function of near tip constraint, the application of a critical value calculated from a test specimen may not match with the actual point of structural failure. Two concerns of primary interest when implementing a two-dimensional approach are: (i) evaluation of the conservativeness of the two-parameter failure locus, and (ii) the geometric limits on test specimens in order to achieve a repeatable failure limit in testing. Similar to single parameter fracture prediction, stress fields surrounding the crack-tip will not maintain two-parameter dominance for loads exceeding deformation limits, and hence this measurement is useful to evaluate limits for test specimens. It has been proposed in recent ASTM standard development that a material dependent limit is practical for surface crack specimens. However, a material based criterion is useful when a minimal number of measurable input parameters are used. For example, a criterion dependent only on the ratio of elastic modulus to yield strength would be desirable if it can be shown that a conservative limit exists as a function of this ratio. This study aims to assess an additional degree of freedom, namely the level of strain hardening, keeping the elastic modulus to yield strength ratio fixed.

Many investigators have addressed the differences in near tip fields for various strain hardening materials, but this literature does not provide a clear description of these fields with respect to the two-parameter fracture predictions for surface crack configurations. O'Dowd (1995) showed the strong constraint dependency on plastic strains near the crack tip for various power-law hardening materials. Constraint or triaxiality directly influences the size and shape of the plastic zone. Lower or negative constraint results in a large plastic zone shifted in the crack growth direction. In an earlier paper, O'Dowd and Shih (1991) showed that as plastic flow propagates through the remaining ligament of a cracked body of finite thickness, the material must have sufficient strain hardening for accurate J–Q formulation. The strain hardening effects of crack tip deformations with respect to the J-integral directly influence the continued existence of a J–Q dominated field with very little influence from constraint and elastic properties.

This study investigates the influence of the strain hardening exponent, defined for a linear plus power law material model, on two-parameter (J–Q) fracture characterization and the associated limitations by presenting near tip stress fields for surface crack tensile geometries. The near tip stresses are referenced by the material specific J–Q family of fields generated with MBL formulations for linear plus power-law materials with strain hardening exponents of $n = 3$ (high strain hardening) and $n = 20$ (low strain hardening) with $E/\sigma_o = 250$. The results from this study are of immediate relevance towards establishing testing standards for surface crack geometries. Methodology for determining the limits of two-parameter characterization for surface cracks are established and multiple techniques are presented.

2. Background

2.1. J–Q theory

J–Q theory has been implemented for the characterization of near tip stress fields for 2D and 3D geometries by many investigators. Wang (2009) shows that the Q parameter as a measure of the difference between the actual opening stress and the small-scale yielding solution is accurate for a range of normalized radial distances ($r/(J/\sigma_o)$) for loads exceeding yield, where the ratio J/σ_o scales with the blunting zone diameter or crack tip opening displacement.

The constraint parameter Q is defined as the difference between the actual hoop stress ($\sigma_{\theta\theta}$) and a reference hoop stress within a cracked body. The hoop stress ($\sigma_{\theta\theta}$) is defined as the normal stress in the direction tangent to a circular region enclosing the crack tip. Fig. 1 gives a definition of the θ direction for the MBL models. O'Dowd and Shih (1991, 1992) showed that the following equation can be used within a range of normalized radial distances, typically $1.5 \leqslant r/(J/\sigma_o) \leqslant 5$ to accurately represent the near crack fields:

$$\sigma_{ij}(r,\theta) = \left[\sigma_{ij}\left(\frac{r}{J/\sigma_o},\theta\right)\right]_{T=0} + Q\sigma_o\delta_{ij} \text{for} -\pi/2 \leqslant \theta \leqslant \pi/2, \tag{1}$$

where the first term is the SSY solution and δ_{ij} is the Kronecker delta. The SSY solution is used over the HRR solution, first proposed by O'Dowd and Shih (1991, 1992), to reduce the radial distance dependency (O'Dowd and Shih, 1994).

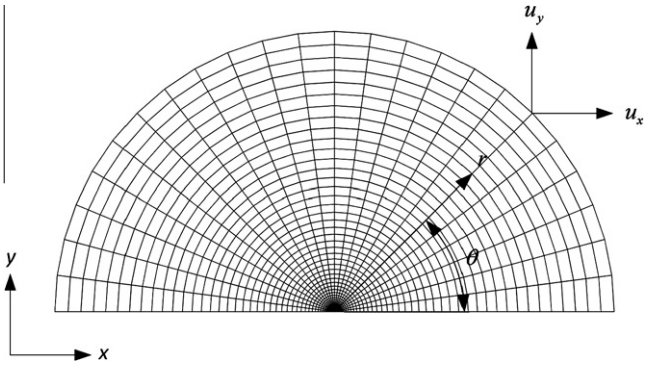

Fig. 1. Modified boundary layer (MBL) model mesh and displacement boundary conditions.

In the analyses presented by Silva et al. (2006), plane-strain results produce relatively unchanged Q values when the normalized radial distance from the crack tip is varied between $1 \leqslant r/(J/\sigma_o) \leqslant 5$. Similarly, three-dimensional crack front fields in surface crack specimens, where the points are embedded entirely in material, there exists a state of plane-strain near the crack tip. Therefore, variations of the normalized radial distance within this range for J-dominant surface crack fields should not change the general trends presented in the analysis or the conclusions derived from them. The Q-parameter is best defined as a fracture parameter when the normalized radial distance equals $2J/\sigma_0$ because this marks the location where cleavage mechanism is triggered ahead of the crack tip (Silva et al., 2006). Therefore, in order to be used in two-parameter fracture characterization, Q is defined as the hoop stress difference in the cracked plane (opening stress or σ_{yy}) at a radial distance equal to $2J/\sigma_o$:

$$Q = \frac{\sigma_{yy} - (\sigma_{yy})_{T=0}}{\sigma_o} \quad \text{at } \theta = 0 \quad \text{and} \quad r = 2J/\sigma_0, \tag{2}$$

A single value of Q represents a material dependent near crack stress field as a function of $r/(J/\sigma_o)$, designated the reference space solutions. Using this definition of constraint, a plane-strain J–Q family of fields is constructed using the MBL finite element formulation. Nevertheless, the relative changes in Q with radial distance (r) when measured at larger deformations, necessitates the investigation of opening stress as a function of normalized radial distance $r/(J/\sigma_o)$. The deformation limit of J–Q dominance may therefore be determined by the relative change of opening stress compared to those predicted at $r = 2J/\sigma_0$ defined by Eq. (1) or when the radial independence of Q cannot be assured (Sharma et al., 1995).

2.2. Modified boundary layer solutions

Determining two-parameter dominance of a test specimen or structure relies on the ability to model idealized stress fields within the characterized range. Where analytical solutions exist to compare stress states in fully elastic cracked bodies, the elastic–plastic fields defined for an arbitrary material must be formulated using MBL finite element models.

The MBL stress field solutions are derived from the existence of an asymptotic plane-strain elastic stress field outside crack-tip plastic zone under contained plasticity. This field is uniquely defined by the elastic parameters (K and T). Contained plasticity is defined as the state in which the plastic zone is on a length scale that is small compared to relevant dimensions. Under these conditions, the J-integral simplifies correlatively to K, and therefore a region exists within the plastic zone that must be defined by the elastic–plastic parameter J and a measure of constraint (T or Q). Moreover, the unique fields described by this state are representative of the stress state in any crack geometry and load configuration that is defined by these parameters. SSY conditions are a special case in the MBL formulation where the stress field measured outside the plastic zone but far from the geometry boundaries is characterized by the first singular term of the Williams Eigen expansion (Williams, 1957; Wang, 1993):

$$\sigma_{ij}(r,\theta) = \frac{K_I}{\sqrt{2\pi r}} f_{ij}(\theta), \tag{3}$$

where K_I is the mode I stress intensity factor.

A material flow curve (σ verses ε), typically defined by uniaxial tension data, and the Poisson ratio are the only variables needed to produce a unique set of MBL reference fields. The MBL solution is therefore a *derived* material property. An accurate MBL reference field should be reproducible when it is independent of K-applied and mesh configuration as long as the formulation follows certain criteria defined in the following section.

The remote tractions for MBL formulation are given by the first two terms of the Williams Eigen expansion (Williams, 1957):

$$\sigma_{ij}(r,\theta) = \frac{K_I}{\sqrt{2\pi r}} f_{ij}(\theta) + T\delta_{1i}\delta_{1j}, \tag{4}$$

where K_I is the mode I stress intensity factor and T is the T-stress. Fig. 1 shows the half-symmetric plane-strain FE mesh used for MBL analysis. The first two terms of the Williams series are applied as displacement boundary conditions to the $r = r_{max}$ outer surface. The corresponding in-plane displacements are given by

$$u_i(r,\theta) = \frac{K_I}{E}\sqrt{\frac{r}{2\pi}}g_i(\theta,\nu) + \frac{T}{E}rh_i(\theta,\nu), \tag{5}$$

where E and ν are material constants and g_i and h_i are the angular variations in displacement caused by elastic singularity fields and T-stresses respectively (Wang and Parks, 1995). The angular variations are defined in plane-strain as

$$g_x(\theta,\nu) = (1+\nu)\cos\left(\frac{\theta}{2}\right)(3-4\nu-\cos\theta), \tag{6}$$

$$g_y(\theta,\nu) = (1+\nu)\sin\left(\frac{\theta}{2}\right)(3-4\nu-\cos\theta), \tag{7}$$

$$h_x(\theta,\nu) = (1-\nu^2)\cos\theta, \tag{8}$$

$$h_y(\theta,\nu) = -\nu(1+\nu)\sin\theta, \tag{9}$$

Plane-strain MBL solutions for elastic–plastic crack tip fields can be obtained by applying these displacements to the outer boundary of the circular crack tip region and varying the T-stress while K_I remains constant. The J-integral is related to the stress intensity factor K_I in plane-strain by

$$J = \frac{1-\nu^2}{E}K_I^2. \tag{10}$$

Abaqus version 6.7 is used to compute the MBL solutions (Dassault Systèmes, 2007a). Fig. 2 shows the near crack opening stress fields predicted by our MBL model for the low strain hardening material ($n = 20$).

Wang (1993) showed that these MBL solutions provided accurate prediction of stress fields in surface crack tension (SC(T)) specimens as characterized by J and T, and that the crack tip fields of the MBL solution far from the outer boundary and outside the crack tip blunting zone should represent those of any crack with the same K_I and T. While an elastically scaled T-stress can be used to accurately predict near tip stress fields up to and exceeding net section yield, the physical meaning of T is lost with the onset of large-scale plastic deformation. Therefore, the Q factor, which is calculable at loads exceeding yield, will be used for this study.

Fig. 3(a) shows the unique relationship between T and Q in the MBL solutions. The near tip reference stress fields are often formulated as a function of constraint Q for constant normalized radial distances. Fig. 3(b) gives these curves for $r/(J/\sigma_o) = 2$, 4, 6, and 8.

2.3. MBL formulation criteria

Modified boundary layer solutions can only be formulated within certain constraint levels. As the compressive constraint stresses (negative T-stress) approach the yield stress, crack tip deformations exceed the contained plasticity limits and no

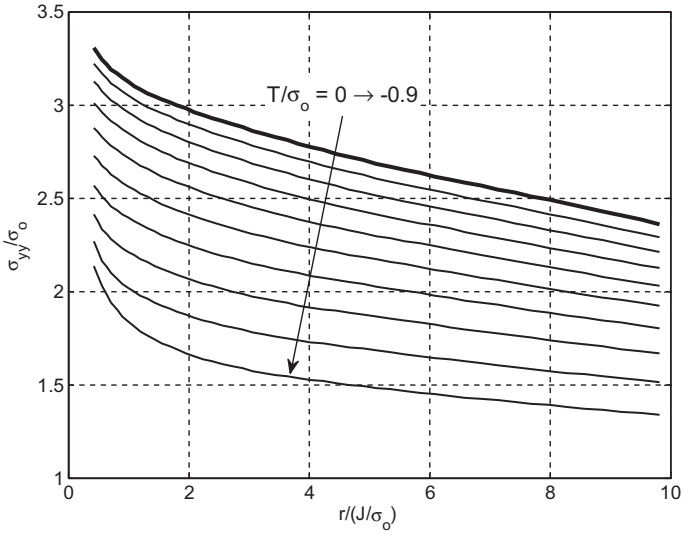

Fig. 2. MBL generated near tip opening stresses as a function of normalized radial distance $r/(J/\sigma_o)$ for a series of negative T-stresses ranging from $T/\sigma_o = 0$ to -0.9.

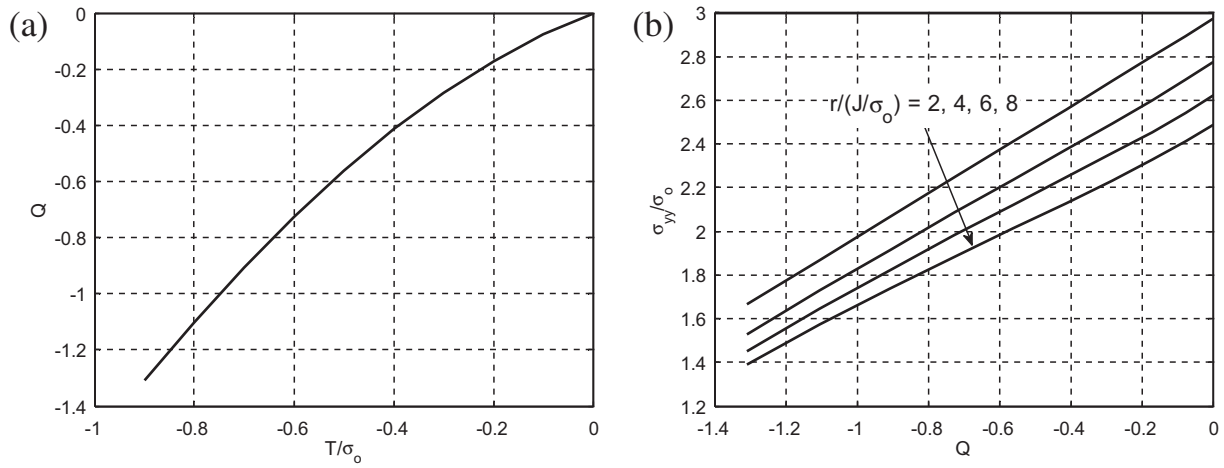

Fig. 3. (a) Relationship between normalized T-stress and Q and (b) reference opening stress as a function of Q for normalized radial distances $r/(J/\sigma_o) = 2$, 4, 6, and 8 for a low strain hardening ($n = 20$) moderate strength $E/\sigma_o = 250$ material.

longer provide an accurate representation of the J predicted field. Literature has shown the applied T-stress limits to be approximately $T = -\sigma_o$, but the actual limits can be determined by close examination of the near tip conditions. When the crack deformations exceed levels necessary for MBL formulation, the elastic–plastic J-integral (J) will deviate from the elastically predicted value (J_{El}), given by Eq. (10), by a considerable amount. This can be formulated as an arbitrary limit where J must not deviate from J_{El} by greater than 10%, as shown below:

$$\left|\frac{J_{El} - J}{J_{El}}\right| \times 100\% \leqslant 10\%. \tag{11}$$

One must also consider the limitation of MBL formulation as a function of applied K. With increasing applied K and the onset of large-scale plasticity at a low level of constraint ($T \to -\sigma_o$), the J-integral deviation, as defined by Eq. (11), increases exponentially. Nevertheless, it is necessary to apply a sufficiently large K to achieve radial data points close to the crack tip. Since K is normalized out for the final reference solutions, repeatability remains solely on adherence to the requirements of Eq. (11), which also ensures deformations below large-scale plasticity. Therefore, the MBL solutions cover the desired level of constraint ($0 \leqslant T/\sigma_o \leqslant -0.9$) and a maximum K is applied such that the error of J at the minimum applied T-stress ($T/\sigma_o = -0.9$) is within the above limits.

3. Specimen configuration and finite element analysis

3.1. Surface cracked tension finite element models

The surface crack tension SC(T) model, shown in Fig. 4, has dimensions $w \times L \times t = 19$ mm $\times$ 19 mm $\times t$, with two thickness values of $t = 1.27$ and 2.54 mm. The crack geometries examined are $a/c = 1.0$ (semi-circular) and 0.40 (semi-elliptical). Table 1 gives a complete list of the four models tested. The crack depth remains constant throughout the analysis at $a = 0.889$ mm. The uniaxial tensile load is applied to the xz face opposite the crack using displacement boundary conditions in the y-direction (u_{yy}). FEA Crack version 3.1.56 (Quest Reliability, 2007) was used to generate the crack mesh and Abaqus version 6.7 (Dassault Systèmes, 2007b) was used for the analysis.

The J-integrals along the crack front are calculated using the domain integral method applied to three dimensions intrinsic to Abaqus. The finite element analyses are made using C3D20R 20-node isoparametric brick elements. At the crack-tip, 20-node collapsed face prismatic elements are used. To allow for crack tip blunting in the elastic–plastic models, the initially coincident nodes at the crack tip are left unconstrained. Fig. 5 schematically illustrates the collapsed face element nodal configuration and boundary conditions for elements with a face in the crack plane in the crack growth direction ($\theta = 0°$). In order to maintain sufficient data points at the desired radial distances, the crack region contains a highly refined mesh consisting of 31 contours around the crack tip and 72 collapsed face elements along the crack front. Fig. 6 shows the crack face mesh with these refinements.

3.2. Mesh convergence study

A preliminary study of mesh refinement was conducted by comparing domain integral (J-integral) values, which tend to be sensitive to mesh refinement, from various models of mesh density. With increasing mesh refinement these factors

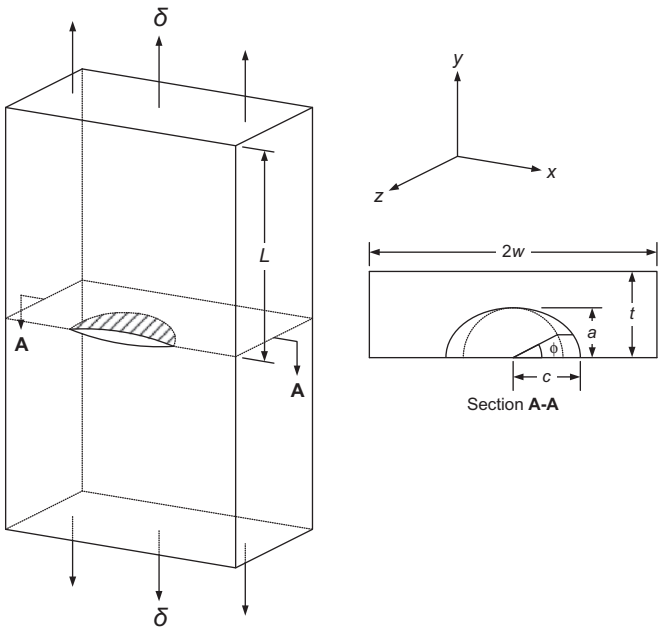

Fig. 4. General surface crack model configuration.

Table 1
Surface crack model dimensions.

Description	Dimensions ($w \times L \times t$)	a/t	a/c	A_{net}/A_o
Semi-circular deep	19 × 19 × 1.27 mm	0.70	1.0	0.974
Semi-circular shallow	19 × 19 × 2.54 mm	0.35	1.0	0.987
Semi-elliptical deep	19 × 19 × 1.27 mm	0.70	0.4	0.936
Semi-elliptical shallow	19 × 19 × 2.54 mm	0.35	0.4	0.968

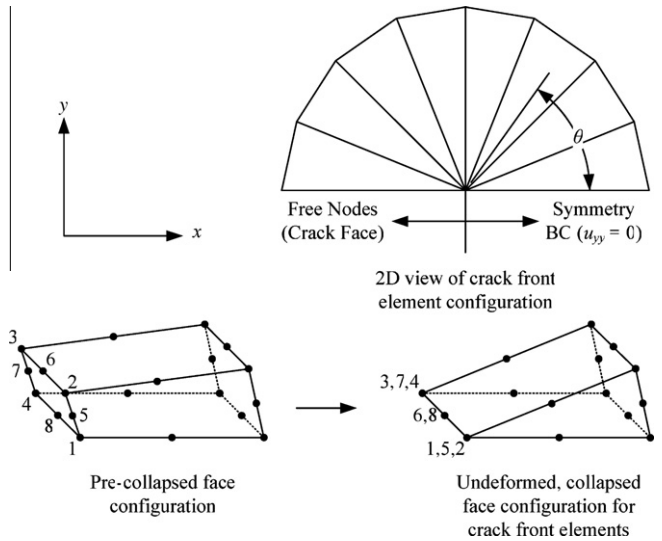

Fig. 5. Example of crack front collapsed face nodal configuration. For elements with a face in the $\theta = 0^\circ$ plane, nodes 2, 3, 5, 6, and 7 are free while displacement $u_{yy} = 0$ for nodes 1, 4 and 8. All other initially coincident nodes are free for remaining elements in the θ direction

converged to stable values. The final mesh resulted in domain integral calculations that varied by a negligible amount ($\Delta(J) < 0.10\%$). The chosen mesh refinement is beyond the level needed for accurate stress and domain integral calculations, but was necessary to achieve sufficient radial data points to assess the opening stress field using interpolation methods.

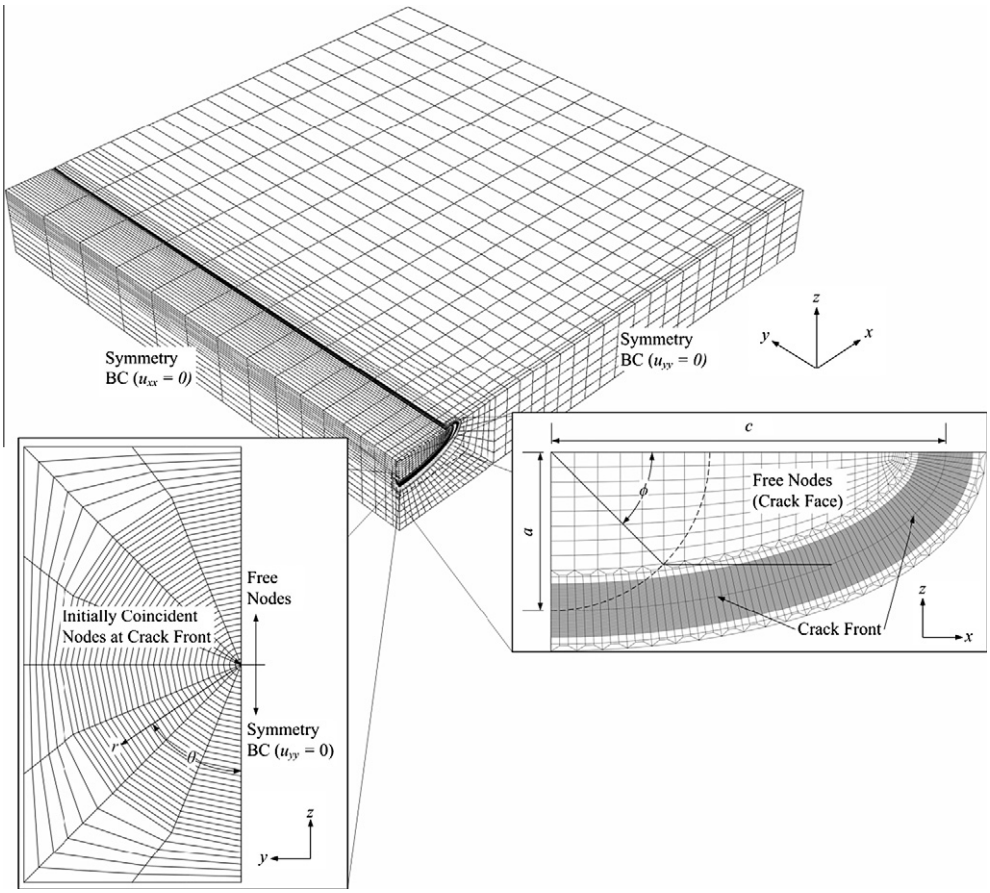

Fig. 6. Finite element surface cracked mesh refinement detail.

Increasing the number of nodes in the radial direction from the crack-tip will decrease the maximum possible error in interpolation within numerical limitations. The near tip stress measurements obtained by a less refined mesh compared accurately to the results from the final mesh refinement (see Fig. 6) when the number of radial points in the coarse mesh used in interpolation is maximized by limiting the range of deformations observed. In other words, an accurate comparison can be made between meshes when the radius of near tip mesh refinement is approximately equal to $10J/\sigma_o$, resulting in the maximum number of stress measurements. Outside this range, the coarse mesh does not contain sufficient data points for a meaningful comparison.

3.3. Element formulation

Crack tip blunting effects can typically be neglected at distances roughly one and a half to twice the crack-tip opening displacement or $1.5J/\sigma_o \rightarrow 2J/\sigma_o$. Inside this distance from the crack tip, it would be necessary to use large-strain analysis (Betegón and Hancock, 1991; Wang, 2009). Linear kinematic element formulation (small-strain) simplifies the analysis because it does not require a finite radius crack-tip and often converges with a relatively coarse mesh. Non-linear kinematic element formulation (large-strain) requires a finite radius crack-tip and therefore mesh convergence is often difficult to achieve. For this investigation, small-strain approximation is used to analyze stress fields outside the crack-tip blunting zone in the surface cracked models. Fig. 7(a) gives an example of how the small strain approximation of opening stresses differ from those calculated using large-strain analysis with a finite radius key-hole mesh configuration at the crack-tip. This figure gives opening stress data from a single edge notched tension (SEN(T)) model ($a/W = 0.20$) with plane-strain boundary conditions at a load $a\sigma_o/J = 40$ using the two linear plus power-law material models described in the next section. Fig. 7(b) gives the percent difference between the large and small-strain results. Percent difference is defined as

$$\%\ \text{Difference} = \frac{\sigma_{yy}^{\text{Large-Strain}} - \sigma_{yy}^{\text{Small-Strain}}}{\sigma_{yy}^{\text{Large-Strain}}} \times 100\%, \tag{12}$$

Both low and high strain hardening materials, $n = 20$ and 3, respectively, achieve 95% opening stress accuracy within the radial distance $r = 2J/\sigma_o$. Additionally, the higher strain hardening material achieves 95% accuracy at a smaller radial distance ($r = 1.5J/\sigma_o$) compared to the model with the low strain hardening material.

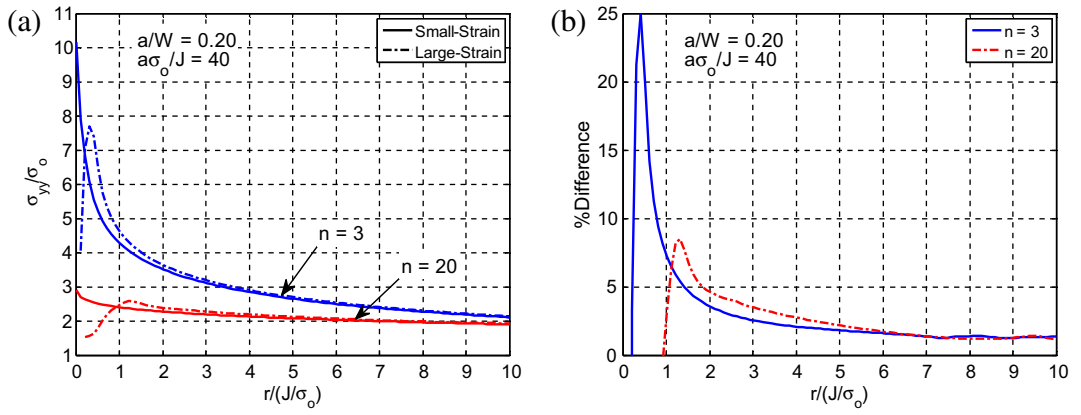

Fig. 7. Data obtained from a single edge notched tensile (SEN(T)) specimen demonstrating the effects of using linear (small-strain) and non-linear (large-strain) kinematic element formulations. (a) Opening stress (σ_{yy}) and (b) percentage difference verses normalized radial distance ($r/(J/\sigma_o)$) is given for a constant load $a\sigma_o/J = 40$.

3.4. Materials

The focus of this analysis is to study the effects of strain hardening on crack tip stress fields relative to MBL solutions. Due to the fully plastic nature of the loadings, the strain hardening is expected to have a significant effect on the stress fields. Material dependent reference solutions are created for each of the elastic–plastic materials tested. Therefore, the predicted stresses should take into account the material strain hardening for loads up to the deformation limits of the geometry. For this study, two linear plus power-law material models shown in Fig. 8 are used to simulate low strain hardening ($n = 20$) and high stain hardening ($n = 3$). This material model correctly defines many actual material flow curve shapes often measured experimentally by a uniaxial tension specimen. The linear plus power-law model is defined by

$$\frac{\varepsilon}{\varepsilon_o} = \frac{\sigma}{\sigma_o} \quad \text{for} \quad \frac{\sigma}{\sigma_o} \leqslant 1, \tag{13}$$

$$\frac{\varepsilon}{\varepsilon_o} = \left(\frac{\sigma}{\sigma_o}\right)^n \quad \text{for} \quad \frac{\sigma}{\sigma_o} > 1, \tag{14}$$

$$\varepsilon_o = \frac{\sigma_o}{E}, \tag{15}$$

where E is the elastic modulus, n is the strain hardening exponent, σ_o is the reference yield stress and ε_o is the yield strain. For this investigation $E = 68.95$ GPa, $\sigma_o = 275.8$ MPa and $\nu = 0.33$ ($E/\sigma_o = 250$). In order to ensure gradual transition from elastic to plastic strains, a circular transition arc region is included (Healy et al., 2009). Eqs. (13) and (14) become:

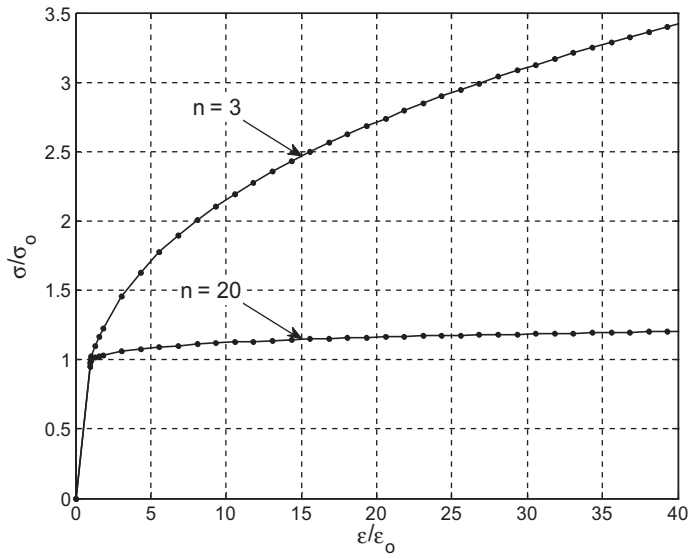

Fig. 8. Linear plus power law material models for the high ($n = 3$) and low ($n = 20$) strain hardening materials used in the surface crack analysis ($E/\sigma_o = 250$ and $\nu = 0.33$)

$$\frac{\varepsilon}{\varepsilon_o} = \frac{\sigma}{\sigma_o} \quad \text{for} \quad \frac{\sigma}{\sigma_o} \leqslant K_1, \tag{16}$$

$$\frac{\varepsilon}{\varepsilon_o} = \varepsilon_{Nc} - \sqrt{r_{Nc}^2 - \left(\frac{\sigma}{\sigma_o} - \sigma_{Nc}\right)^2} \quad \text{for} \quad K_1 \leqslant \frac{\sigma}{\sigma_o} \leqslant K_2, \tag{17}$$

$$\frac{\varepsilon}{\varepsilon_o} = \left(\frac{\sigma}{\sigma_o}\right)^n \quad \text{for} \quad \frac{\sigma}{\sigma_o} > K_2, \tag{18}$$

where $(\varepsilon_{Nc}, \sigma_{Nc})$ is the center and r_{Nc} is the radius of the circular arc in normalized space $(\varepsilon/\varepsilon_o, \sigma/\sigma_o)$. K_1 is the lower limit of the transition region, which is set at $K_1 = 0.95$, and K_2 is upper limit. Therefore, $K_1\sigma_o$ defines the elastic limit of the material. By ensuring the slopes at the points of transition (K_1, K_2) are continuous, the remaining variables can be calculated $(\varepsilon_{Nc}, \sigma_{Nc}, r_{Nc}, K_2)$. The flow curve smooth transition region is primarily implemented to aid in the convergence of the incremental plasticity solver. Additionally, the curve defined by the latter equations represents more accurately the inherently smooth experimental curve from uniaxial specimens. The existence of the transition region has little effect on the results and is merely a numerical artifact. The material curve is discretized into stress and plastic strain inputs for the FEA model with a high concentration of points in the region of initial plastic strains. The material inputs are shown as solid points in Fig. 8. Incremental theory plasticity, which follows the von Mises yield criterion (J_2 flow rule), is used for this analysis.

3.5. Near tip stress field analysis and plastic collapse

The near tip stress fields are analyzed in the cracked plane along the vector normal to the crack front in the growth direction. The radial distance r from the crack front is normalized by J/σ_o which gives a length scale comparable with MBL solutions. The nodal opening stress values are used along with cubic spline interpolation to determine the near tip stress distribution. From this curve, the value of Q is determined with Eq. (2). The unique relationship of Q to a specific near tip field provides the reference solution for comparison.

Fig. 9(a) and (b) provide examples of near tip opening stress fields as a function of normalized radial distance $(r/(J/\sigma_o))$ for high strain hardening and low strain hardening materials respectively. The J–Q MBL predicted stress field and the neutral constraint (SSY) stresses are given as references for the actual stress state in a surface crack model with $a/c = 1.0$ and $a/t = 0.35$ at crack depth ($\phi = 90^\circ$) for a far field load $\sigma_\infty = \sigma_o$. Two processes exist by which near tip stress field parameterization is lost. First, single parameter dominance is limited in low constraint geometries by a loss of constraint or triaxiality near the tip resulting in significant deviation from the SSY solution, even under contained plasticity. Secondly, two-parameter dominance is limited by the amount of deformation at the crack tip and the subsequent shape change and/or rapid relaxation of the fields compared to those predicted by MBL solutions. This process is referred to as plastic field collapse. Because the stress fields in J–Q characterization are referenced to a point near the crack tip ($r = 2J/\sigma_o$), field collapse is measured as difference at larger radial distances or slope variation from the predicted field.

4. Results and discussion

4.1. J-integral and Q

Fig. 10(a) and (b) show the J-integral as a function of crack angle ϕ at a constant average net section stress $\sigma_{Net} = \sigma_o$ for the semi-circular and semi-elliptical cracks respectively. Geometries with lower strain hardening materials exhibit greater redistribution of stresses near the crack tip resulting in higher J-integrals and crack tip deformations. Similarly, higher strain hardening results in smaller plastic zones because the material inside the plastic zone is capable of supporting higher stresses, therefore less stress redistribution is necessary. Fig. 10 gives a clear example of these trends at a constant average net section stress for all the surface crack models tested. It is necessary when ϕ becomes small (near the free surface) to ignore angles $\phi < 5^\circ$ because a J-dominated field will only be present at near crack points embedded entirely in material (Wang, 2009). Therefore, figures that are a function of ϕ show data for angles $\phi > 5^\circ$.

Fig. 11(a) and (b) give Q, defined in Eq. (2), as a function of crack angle ϕ at a constant average net section stress $\sigma_{Net} = \sigma_o$ for the semi-circular and semi-elliptical cracks respectively. The models with the lower strain hardening material has lower (more negative) Q factors for a given far field load. Near tip stress field reduction associated with constraint loss (more negative Q factors) is a result of redistributions in the plastic zone which is amplified by the lack of strain hardening. The combination of stress redistribution and relaxation associated with constraint loss results in a greater degree of crack tip deformations in the low strain hardening cases compared to the high strain hardening cases. This postulate will be further supported in near tip stress field analysis.

Much of the analysis is done for the case of $\phi = 30^\circ$ for both aspect ratios $a/c = 1.0$ and 0.40. This angle is close to those predicted to be the most critical based on the criteria proposed by Leach et al. (2007) in which the critical crack extension angle corresponds to the maximum product of the average opening stress over the plastic zone and the J-integral. This criterion roughly corresponds to the angles for which J and Q are maximum, which can be estimated from Figs. 10 and 11, respectively. Experimentally, the critical angle analysis shows considerable scatter. Therefore, the angles shown here will

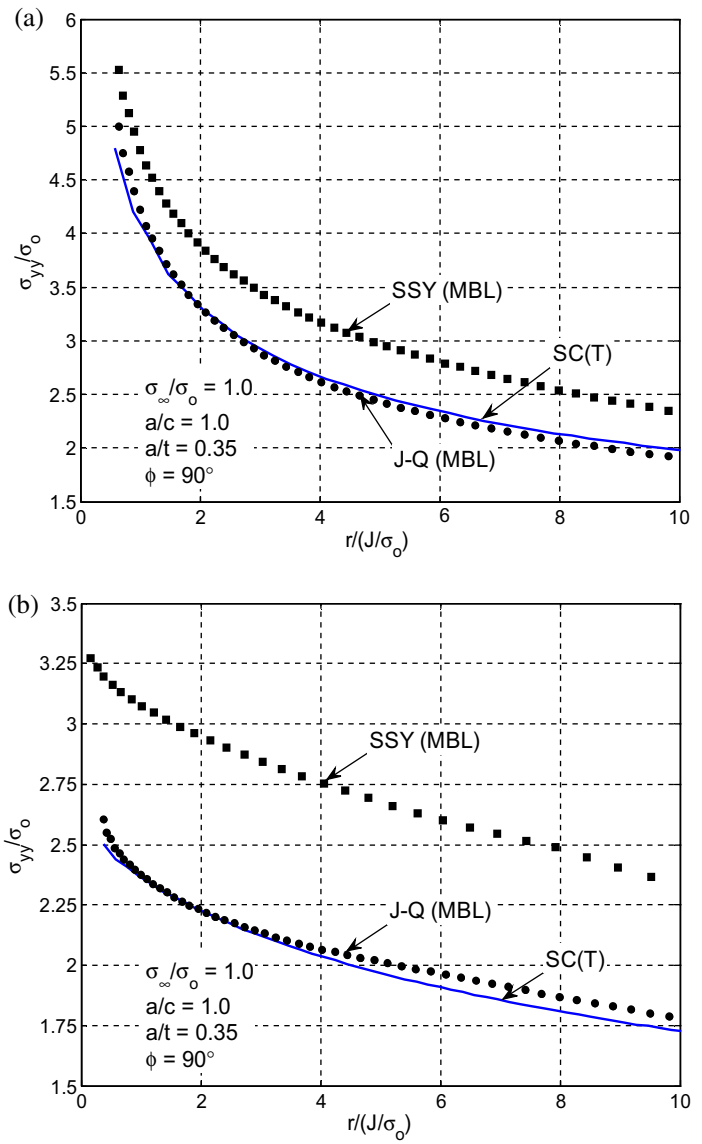

Fig. 9. Examples of the near tip opening stress fields at a constant far field stress $\sigma_\infty = \sigma_o$ as a function of normalized radial distance $r/(J/\sigma_o)$ for a semicircular surface crack (SC(T)) ($a/c = 1.0$ and $a/t = 0.35$) with the zero constraint small-scale yielding (SSY) and the constraint corrected J–Q predicted fields shown as solid points for materials with (a) $n = 3$ and (b) $n = 20$.

not necessarily be the most critical in terms of crack growth, but should represent the general trends within the critical region. Other angles show similar trends but the detailed analyses are not shown here.

Fig. 12(a) and (b) show the local deformation factor $l\sigma_o/J$ at crack angle $\phi = 30^\circ$ as a function of normalized average net section stress σ_{Net}/σ_o for the semi-circular and semi-elliptical cracks respectively. The local deformation parameter has been used by many investigators as a measure of load. This parameter is valuable in geometric limit analysis for fracture parameterization because it includes a measure of characteristic length (l) and the J-integral. A material dependent limit, based on the local deformation factor, may exist that relates the J-integral at field collapse to the lengths of the specimen. For this study, crack depth a is used to represent the characteristic length of the specimen ($l\sigma_o/J = a\sigma_o/J$), and therefore cannot be directly related to a geometrically independent limiting factor, but can be used to evaluate the relative characteristic lengths between specimens. All subsequent references to the local deformation factor will be in the form $a\sigma_o/J$.

At loads below average net section yield, the near tip conditions show only moderate plasticity and the differences in J are only due to geometric effects on crack mouth opening. The apparent drop in $a\sigma_o/J$ on a log scale at an average net stress approximately yield ($\sigma_{Net} \approx \sigma_o$) is a result of the non-linear increase in J as the near tip fields proceed to large-scale yielding. At a local deformation of $a\sigma_o/J = 40$ (used in following sections) the near tip fields can be characterized by either large-scale yielding or plastic field collapse.

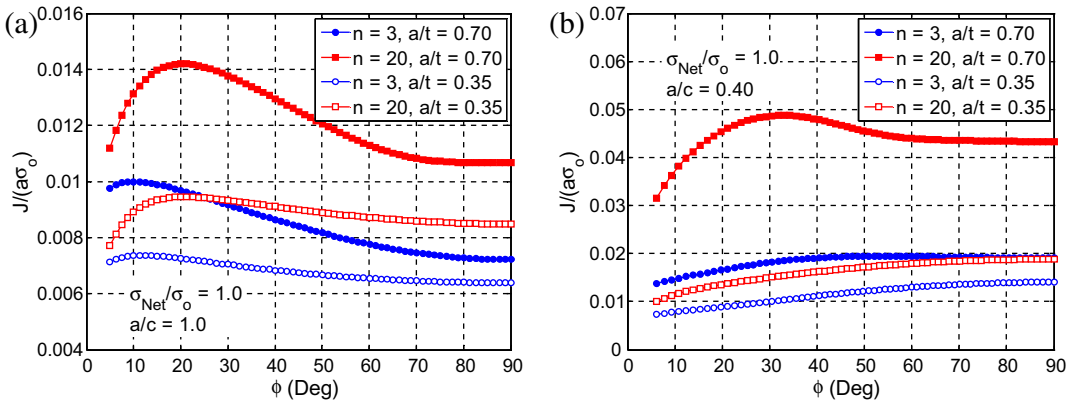

Fig. 10. *J*-integrals as a function of crack angle ϕ at a constant average net section stress $\sigma_{Net} = \sigma_o$ for $a/t = 0.70$ and 0.35 and aspect ratios $a/c = 1.0$ (a) and 0.40 (b).

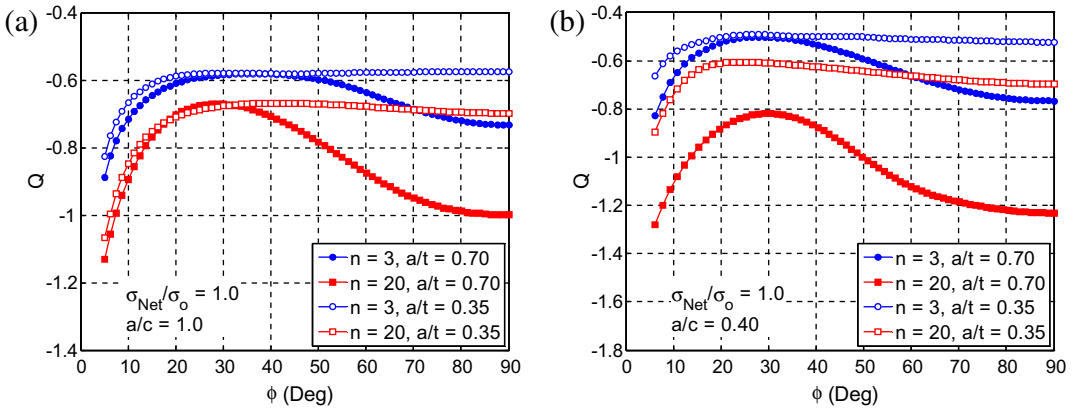

Fig. 11. *Q* as a function of crack angle ϕ at a constant average net section stress $\sigma_{Net} = \sigma_o$ for $a/t = 0.70$ and 0.35 and aspect ratios $a/c = 1.0$ (a) and 0.40 (b).

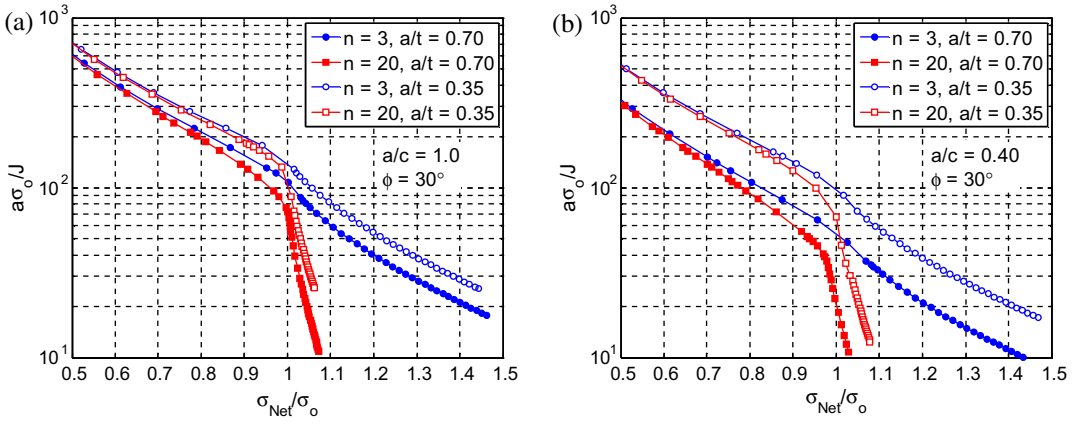

Fig. 12. Local deformation factor $a\sigma_o/J$ at crack angle $\phi = 30^\circ$ as a function of normalized average net section stress σ_{Net}/σ_o for $a/t = 0.70$ and 0.35 and aspect ratios $a/c =$ (a) 1.0 and (b) 0.40.

4.2. Crack tip deformation

O'Dowd and Shih (1991) showed that the relationship between CTOD and *J* depends strongly on the strain-hardening exponent and weakly on elastic properties and *Q*. Similarly, Chiodo and Ruggieri (2010), in a study on surface cracks in pipes under bending, showed this relationship is independent of geometry within easily achievable limits. In a low strain-harden-

ing material, the crack tip deformations are dominated by large plastic strains. Conversely, near tip field with a high strain hardening material has greater resistance to deformation because the material is capable of carrying higher stresses in the plastic zone resulting in tip deformations with a larger portion attributed to elastic strains.

The finite element models used in this analysis contain collapsed face prismatic elements at the crack tip. In order to simulate crack tip blunting the unconstrained nodes are allowed to separate during loading. The out-of-plane displacement of this blunting is used to estimate the level of crack tip deformation. Referring to Fig. 13, u_y is the out-of-plane (opening) displacement of the crack face measured from the vector perpendicular to the crack front in the crack plane. In our analysis, u_y will be used to denote crack tip blunting, calculated as the maximum out-of-plane nodal displacement in the initially coincident nodes at the crack tip. For models with the low strain-hardening material, this measurement of crack tip opening is similar to CTOD taken at the intersection of a 90° vertex with the crack flanks, as shown in Fig. 13 (Anderson, 2004). In high strain hardening material, the crack tip blunting displacement (u_y) will underestimate CTOD because tip deformations are more distributed along the crack face. In low strain hardening material, crack opening is more localized at the tip, resulting in $2u_y \approx$ CTOD. Therefore, u_y can be used to isolate the crack tip deformation/blunting with a higher dependency on plastic strains.

Fig. 14(a) and (b) show the crack tip blunting displacement (u_y) as a function of normalized J-integral (J/σ_o) at crack angle $\phi = 30°$. Similar to the abovementioned references, the slope ($u_y/(J/\sigma_o)$) of the relationship is more or less constant for each

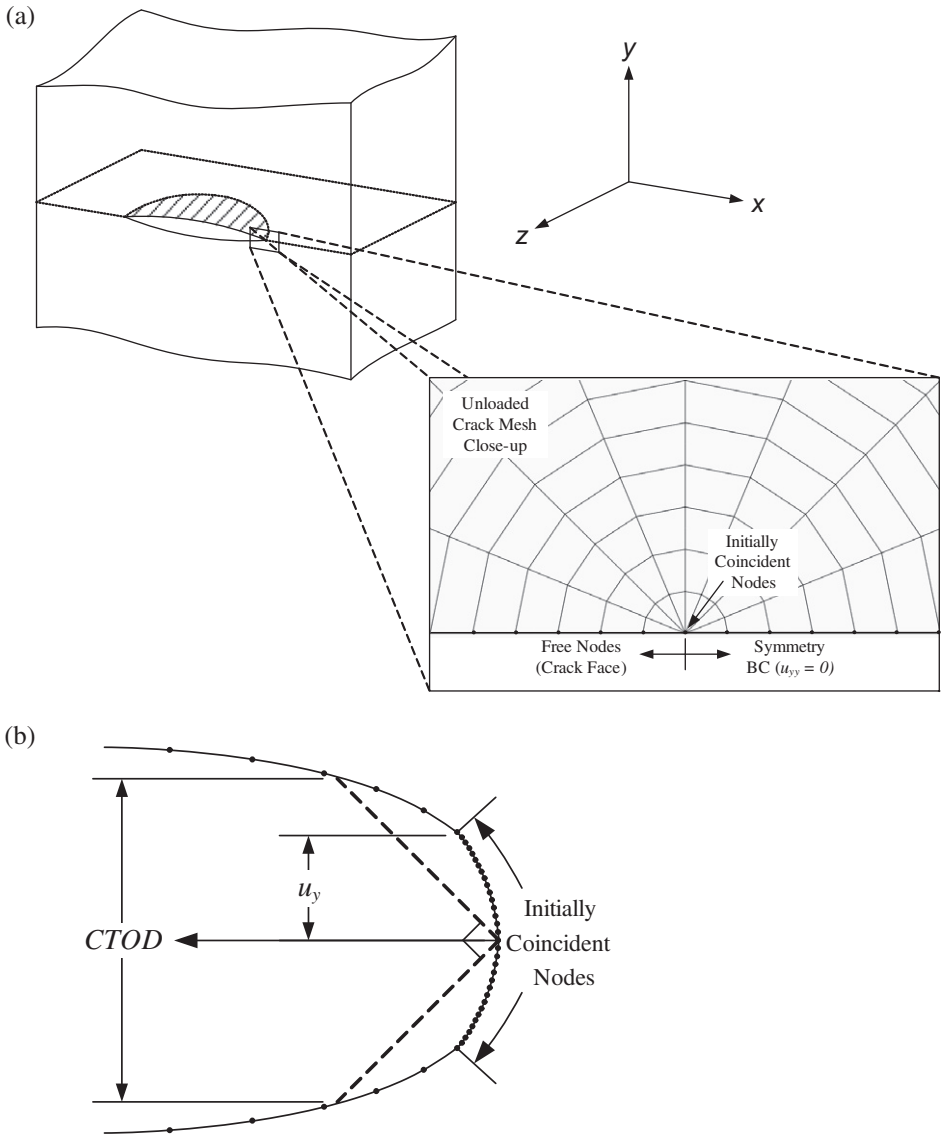

Fig. 13. Schematic representation of (a) crack-tip mesh configuration and (b) the relationship between the crack-tip blunting displacement (u_y) and CTOD in a typical crack-tip from this analysis.

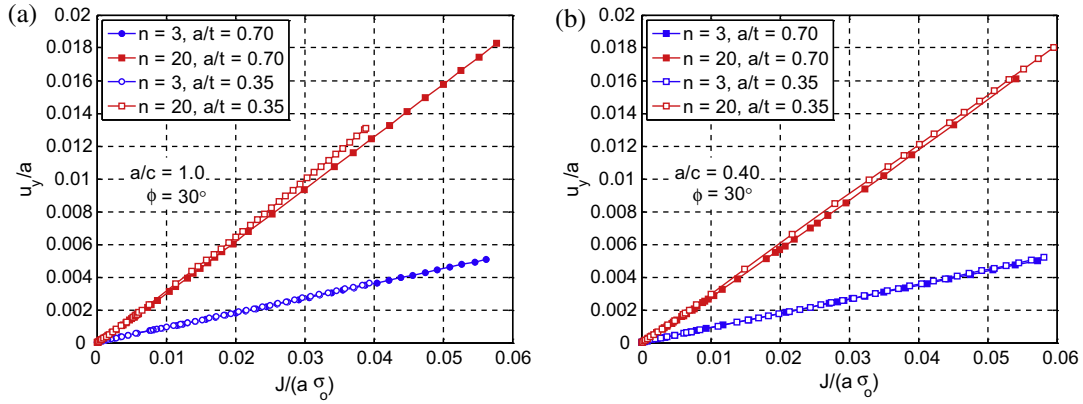

Fig. 14. Crack tip blunting displacement u_y verses J-integral at crack angle $\phi = 30^\circ$ for $a/t = 0.70$ and 0.35 for aspect ratios (a) $a/c = 1.0$ and (b) 0.40.

material and seemingly independent of geometry. The models with the low strain hardening material have significantly higher values of $u_y/(J/\sigma_o)$ compared to the models with the high strain hardening material. This data not only shows that there is an increase in near tip deformation with lower strain hardening but also that the proportion of tip deformation to J is significantly influenced by strain hardening. The higher ratio will have significant implications for near tip stress field analysis with MBL solutions which are functions of the J-scaled length parameter $r/(J/\sigma_o)$. The direct proportionality of J to the physical location of measurement r for a constant $r/(J/\sigma_o)$ makes the proportion of J to near tip deformations important.

The ratio of crack tip deformations to J has a significant effect on the physical meaning of the normalized radial distance and the local deformation factor. For example, a constant normalized radial distance $r/(J/\sigma_o) = 4$ corresponds to a physical distance that is four times the crack tip deformation predicted by J/σ_o while a constant local deformation factor $a\sigma_o/J = 80$ corresponds to a state where the crack depth a is eighty times the crack tip deformation predicted by J/σ_o. Wang and Parks (1995) estimated this factor to be $J/\sigma_o \approx 2\text{CTOD} \approx 4u_y$ for a linear plus power law material with $n = 10$. For our materials, $J/\sigma_o \approx 11u_y$ and $J/\sigma_o \approx 3u_y$ for $n = 3$ and 20 respectively.

MBL solutions have the same relationship between crack tip deformation and J, but by definition, crack tip blunting has no effect on the near tip fields in MBL formulation. It is only when crack tip blunting (u_y) is large compared to the characteristic length of the specimen that the effects on the near tip fields are significant.

It is often useful to summarize crack tip deformation effects by examining the near tip fields at a constant normalized radial distance from the crack tip. Given these material dependent slopes, stress fields will be measured closer to the crack tip proportional to the blunting effected zone for models with the low strain hardening material. However, this should not be interpreted to mean that the actual limits of fracture parameterization are better represented by the physical crack tip deformation such as u_y or CTOD. It is entirely necessary to provide load/deformation limits as a function of the measured fracture parameters, in this case J.

4.3. Near tip opening stress fields

The most obvious and significant comparison with regard to the crack driving force is of the opening stresses in the crack plane ($\theta = 0^\circ$). This section presents the near tip opening stresses from the surface crack models as functions of net section loads and local deformations. All the stresses are normalized by the stress predicted by the modified boundary layer solutions at the corresponding Q factor (σ_{MBL}).

Fig. 15(a)–(d) show the opening stresses normalized by the MBL J–Q predicted stresses at a radial distance $r = 4J/\sigma_o$ as a function of average net-section stress for surface crack specimen dimensions $a/c = 1.0$ and 0.40 and $a/t = 0.70$ and 0.35. The influence of far-field and net section loads and crack tip deformations for limit methodology, which looks at quantifiable deviations from the predicted curve, can be effectively summarized by examining the near tip fields at a constant normalized radial distance from the crack tip. As discussed in the finite element mesh section, the data presented at a constant normalized radial distance is limited to the radius of mesh refinement. When J increases, the physical point of measurement for a constant $r = 4J/\sigma_o$ increases.

The radial independence of Q for the range $1.5 \leqslant r/(J/\sigma_o) \leqslant 5$ corresponding to a hydrostatic shift in stresses, given by Eq. (1), may mark the limit of the usefulness of Q as a ductile fracture parameter. The analysis of opening stresses at a greater radial distance, say $r = 4J/\sigma_o$, is essentially a measure of the radial independence of Q, defined in Eq. (2), providing the MBL solutions represent a radial independent measure of Q (Sharma et al., 1995).

In structures experiencing large loads during normal operations, a load based limit analysis is useful. This type of methodology is restricted to specific geometries and materials combinations and lack the robust features desired in a deformation limit methodology. English et al. (2010) showed the validity of two-parameter characterization in bonded structures expe-

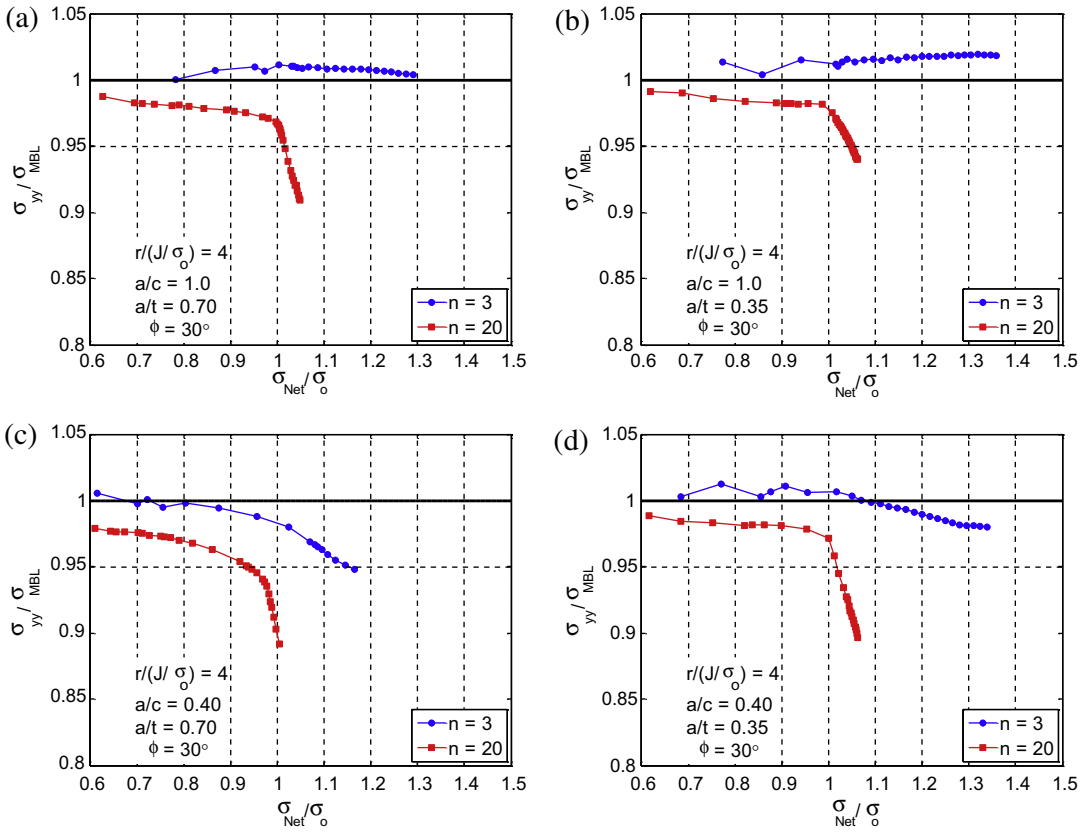

Fig. 15. Opening stresses normalized by the MBL predicted stresses at a constant normalized radial distance $r/(J/\sigma_o) = 4$ and crack angle $\phi = 30^\circ$ as a function of normalized average net section stress σ_{Net}/σ_o for all the surface cracked models implemented.

riencing far-field plasticity and the importance of load based limit determinations. Wang and Parks (1995) also address the importance of load based limit determination for engineering applications.

Although the calculation of a specific stress load at collapse for limit determination is not relevant when comparing to different strain hardening materials, the trends in relative opening stress at net section yield is useful in determining the dependence on plastic flow through the remaining ligament. All the low strain hardening models, except the semi-elliptical crack in the thin plate ($a/c = 0.40$, $a/t = 0.70$), show a clear decrease in near tip opening stresses relative to those predicted by MBL solutions at average net section yield. The deviation from the predicted field at loads less that yield in the semi-elliptical crack in the thin plate ($a/c = 0.40$, $a/t = 0.70$) with the low strain hardening material is associated with the rapid loss of constraint at loads approaching yield, see Fig. 11(b). Similarly, this geometry with the high strain hardening material is the only one to exhibit plastic collapse at the loads tested with all other models maintain the predicted field through net section yield.

Similar to the results shown in the previously referenced work, the deeply cracked structures ($a/t = 0.70$) exhibit less accurate fields for lower loads in both materials tested. In addition, the elliptical crack ($a/c = 0.40$) also demonstrates lower loads for accurate characterization for both materials. The results based on geometric differences stem from a change in characteristic length of the specimen. Essentially, a small crack ($a/c = 1.0$) in a thick specimen ($a/t = 0.35$) should exhibit the highest level of allowable load before initiation of stress field collapse due to excessive deformation. These observations will be further supported by viewing opening stresses as function of the local deformation parameter.

Fig. 16(a)–(d) show the opening stress normalized by the J–Q predicted stresses at a radial distance $r = 4J/\sigma_o$ as a function of local deformation factor $a\sigma_o/J$ for surface crack specimen dimensions $a/c = 1.0$ and 0.40 and $a/t = 0.70$ and 0.35. Similar to crack tip opening displacement (CTOD), the parameter $a\sigma_o/J$ gives insight into the physical deformations near the crack tip. From Fig. 14, it is shown that the ratio of near tip deformation to the normalizing parameter J/σ_o is material dependent. The lower strain hardening materials are shown to have larger near tip deformations for a constant J-integral. Fig. 16 demonstrates that the increase in relative near tip deformations influences the stress fields. In Fig 16 (c) ($a/c = 0.40$, $a/t = 0.70$) the precise influence on geometric limit determination is clearly demonstrated in the case with lowest characteristic length (the lowest remaining net section area). The data shows the stress fields for both high and low strain hardening materials deviating from the predicted stress fields by greater than 5%. All geometries demonstrate this trend, but only this model gives a clear limit. The high and low strain hardening models show deviation from the predicted stresses by greater than 5% at $a\sigma_o/J = 25$ and 50 respectively.

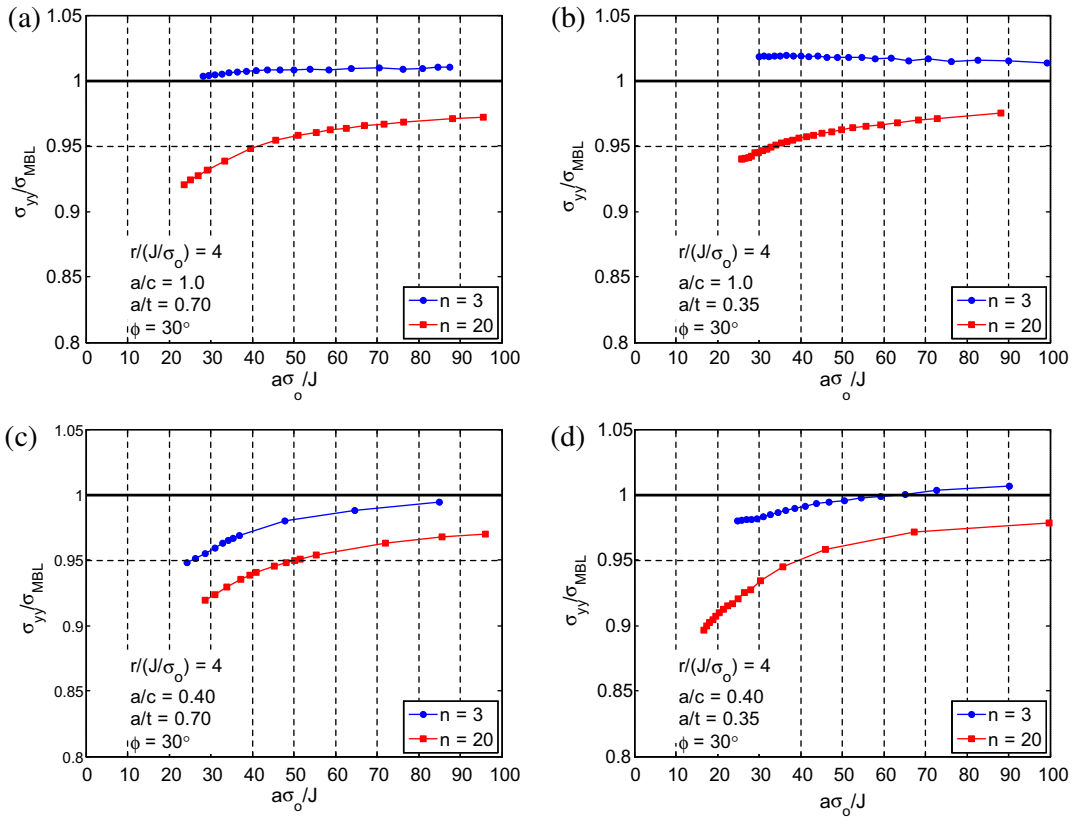

Fig. 16. Opening stresses normalized by the MBL predicted stresses at a constant normalized radial distance $r/(J/\sigma_o) = 4$ and crack angle $\phi = 30^\circ$ as a function of local deformation factor $a\sigma_o/J$ for all the surface cracked models implemented.

The geometric limits are not necessarily defined at a constant radial distance of $r/(J/\sigma_o) = 4$ with a 5% deviation. A criterion for the deformation limits of near tip stress fields based on MBL formulation is debatable and may be better determined experimentally. Nevertheless, for limitation methodology in which J/σ_o is used to normalize both radial distance ($r/(J/\sigma_o)$) and deformation ($a\sigma_o/J$), the plastic properties of the material, in this case the strain hardening exponent, must be accounted for.

For determining relative geometric effects on prediction limits as a function of local deformation, it is important to address differences in net section areas. The ratios of net section area of the remaining ligament (A_{net}) to total nominal area (A_o) are given in Table 1. The relative differences in net section area correlate with the level of local deformation at field collapse in the low strain hardening models. With lower remaining sectional area, the allowable local deformation at collapse decreases (higher limiting $a\sigma_o/J$). Although crack tip deformation in the high strain hardening models is not sufficient to cause significant deviation from the predicted field at this radial distance, the trend of decreasing relative stress is still seen as a function of reducing net section area.

The accuracy of J–Q characterization and the radial independence of Q are measured by the relative difference between a reference state and the field within a near tip zone where both cleavage and ductile fracture mechanisms are active and outside the area where finite strain effect is significant, approximately $1.5 \leqslant r/(J/\sigma_o) \leqslant 5$ (Wang, 2009). For the previous plots, Q is defined at $r = 2J/\sigma_o$, which serves as the reference state, and measurements of the relative differences are taken at $r = 4J/\sigma_o$. This type of analysis is useful for deformation limit methodology, but in order to address the radial extent of J–Q dominance, the opening stresses as a function of normalized radial distance are plotted at a constant load. Fig. 17(a)–(d) show the opening stress as a function of normalized radial distance $r/(J/\sigma_o)$ for a load $a\sigma_o/J = 40$ (large deformation) on a logarithmic scale for all the surface cracked models implemented. The axes are typically shown as logarithms to enhance resolution and simplify slope analysis. The reference solutions and ±5% deviation curves are shown as solid points and dotted lines respectively.

For this method of analyzing near tip fields, the limit of J–Q dominance can be defined by the load at which part of the stress field within the range specified above ($1.5 \leqslant r/(J/\sigma_o) \leqslant 5$) deviates from the predicted curve by greater than 5%. Note that the points that fall $r/(J/\sigma_o) \leqslant 1.5$ may be questionable due to small strain approximations. At the load shown here all the models with the low strain hardening material have lost J–Q dominance while all the models with the high strain hardening material maintain dominance for radial distances $r/(J/\sigma_o) \geqslant 5$.

Fig. 17(b) shows a slight increase of relative near tip opening stresses at large normalized radial distances. This phenomenon is most likely due to far-field effects. The far-field stresses are significant in the $n = 3$ cases because a higher load is needed to

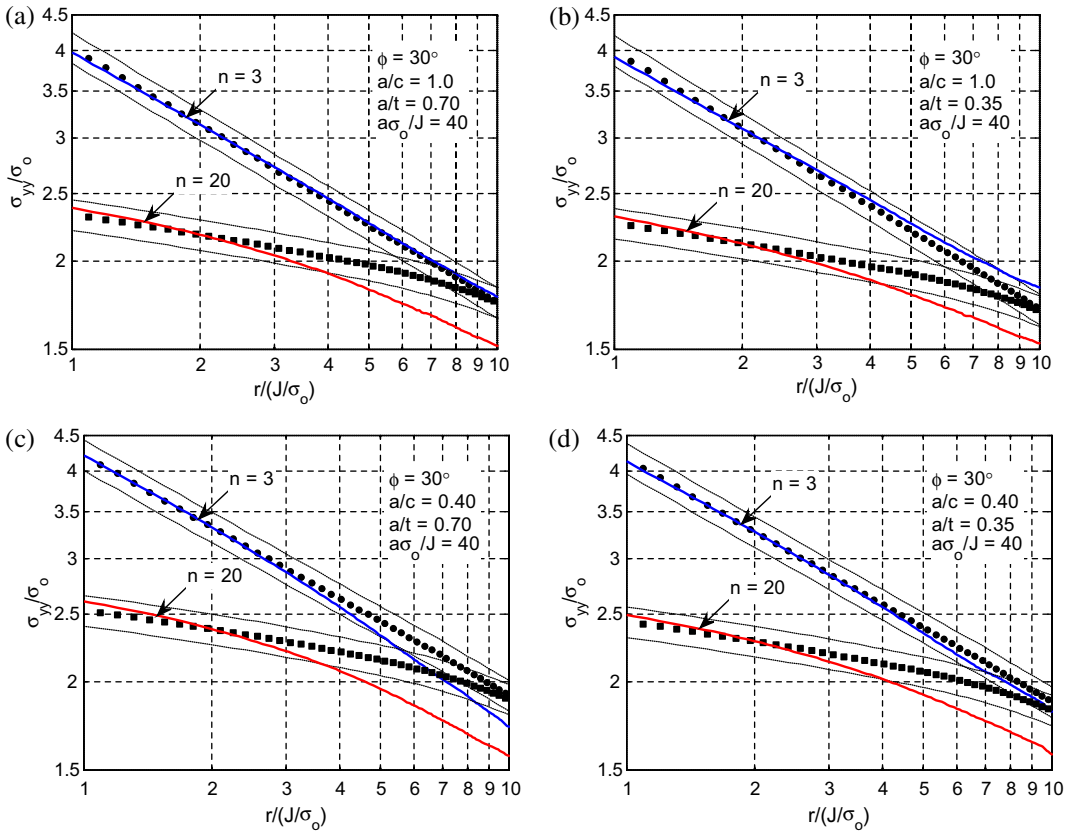

Fig. 17. Opening stresses at an angle $\phi = 30^{\circ}$ as a function of normalized radial distance $r/(J/\sigma_o)$ for a load $a\sigma_o/J = 40$ (large deformation) shown on a logarithmic scale for all the surface cracked models implemented. The reference solutions and 5% deviation curves are shown as solid points and dotted lines, respectively.

achieve the constant local deformation factor (see Fig. 12). Similarly, the thicker models have greater resistance to crack opening as a function of far-field loads. These factors only partially affect near tip stress field analysis and are typically negligible because even at large deformations the near tip fields are still dominated by J and Q within $r/(J/\sigma_o) < 8$.

Fig. 18(a) and (b) show the opening stress normalized by the J–Q predicted stresses at a radial distance $r = 4J/\sigma_o$ and local deformation factor $a\sigma_o/J = 40$ as a function of crack angle ϕ for surface crack specimen dimensions $a/c = 1.0$ and 0.40, respectively. In general, the opening stress fields in the geometries with the high strain hardening material show two-parameter dominance, measured as the percent deviation from the perfectly predicted line ($\sigma_{yy}/\sigma_{MBL} = 1$), equal to or greater than the low strain hardening material. However, for angles closer to crack depth ($\phi > 40^{\circ}$), the differences between material models are diminished. The actual deformation limits at plastic collapse are not clearly shown for these angles; therefore, postulates

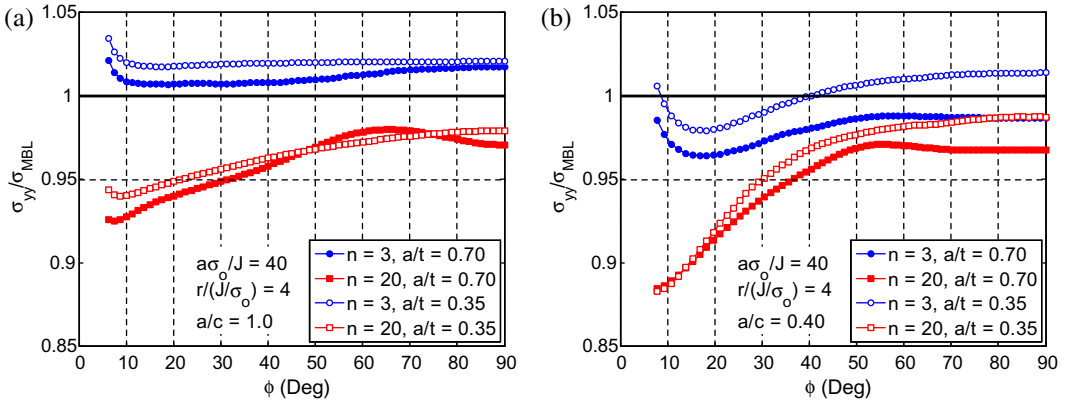

Fig. 18. Opening stresses normalized by the MBL predicted stresses at a constant normalized radial distance $r/(J/\sigma_o) = 4$ as a function of crack angle ϕ for load $a\sigma_o/J = 40$ (large deformation) for cracks with aspect ratios $a/c = 1.0$ (a) and 0.40 (b).

about strain hardening effects on J–Q dominance limits are not possible. Nevertheless, the following observation can be made for loads resulting in a local deformation factor ($a\sigma_o/J \leqslant 40$). Geometries with the low strain hardening material exhibit plastic field collapse at levels of deformation lower than or equal to those found with the high strain hardening material in the surface cracked uniaxial tension geometry.

5. Conclusions

Surface cracks often play a critical role in terms of limiting structural load and life. The near tip constraint conditions of a surface crack must be accounted for in order to evaluate failure conditions. Recent ASTM standard development for surface cracked specimens has favored a material dependent limit that leads to conservative estimates. This study assesses the level of strain hardening as a material limit while keeping the elastic modulus to yield strength ratio constant. The near tip stress fields in a surface cracked metallic plate loaded in uniaxial tension for loads exceeding net-section yield are referenced to material specific J–Q predicted plane-strain modified boundary layer stresses for materials with strain hardening exponents from $n = 3$ (high strain hardening) to $n = 20$ (low strain hardening). The results from this study are of immediate relevance towards establishing testing standards for surface crack geometries. Methodology for determining the limits of two-parameter characterization for surface cracks are established and multiple techniques are presented. Important conclusions are enumerated below:

(a) Strain hardening level has to increase when plastic flow progresses through the remaining ligament for surface cracks under tension, to maintain the predicted field. High strain hardening materials maintained J–Q predicted fields for considerably higher levels of deformation compared to low strain hardening material.
(b) A radially independent Q-parameter, that is applicable to ductile fracture prediction, cannot be measured for the low strain hardening material at larger deformations ($a\sigma_o/J \approx 40$) within a range where both cleavage and ductile fracture mechanisms are present while the high strain hardening material maintained dominance at radial distances including and exceeding the damage zone.
(c) For the low strain hardening material the limit of J–Q dominance and a radial independent measure of Q was a function of remaining net section area.
(d) The local deformation parameter, $l\sigma_o/J$, is a relative measure of near tip deformation limits as a function of both geometry and material properties.
(e) Excessive relaxation at the crack tip results in a nonlinear decrease in the measure of constraint Q. Hence, geometries with a low strain hardening material can exceed the MBL predictable limit due to plastic stress field collapse, leading to a loss of fracture parameterization.
(f) The geometric deformation limit of near tip stress field characterization is proportional to the level of stress the material is capable of carrying within the plastic zone.

A simplified deformation limit criteria may be applicable if the strain-hardening exponent is restricted within a range. The low strain hardening material may be used to provide a clear upper limit to the exponent. It is not recommended however that a deformation limit standard be implemented without addressing the significant effects of strain hardening in standard development or explicitly stated in the standard.

Acknowledgements

The authors express their appreciation for the research support provided by Dr. Phillip A. Allen and others at the NASA Marshall Space Flight Center (MSFC). Ongoing, unpublished research at MSFC concerning the deformation limits for surface crack testing laid the foundation for many of the analytical tools and techniques used in this study.

References

Anderson, T.L., 2004. Fracture Mechanics: Fundamentals and Applications, third ed. CRC Press, Boca Raton.
ASTM, 2006, Standard Test Method for Measurement of Fracture Toughness, pp. E1820-06.
Bai, Y., Wierzbicki, T., 2008. A new model of metal plasticity and fracture with pressure and lode dependence. Int. J. Plasticity 24, 1071–1096.
Betegón, C., Hancock, J.W., 1991. Two-parameter characterization of elastic–plastic crack-tip fields. J. Appl. Mech. 58, 104–110.
Chao, Y.J., Zhu, X.K., 2000. Constraint-modified J–R curves and its application to ductile crack growth. Int. J. Fracture 106, 135–160.
Chiodo, M.S.G., Ruggieri, C., 2010. J and CTOD estimation procedure for circumferential surface cracks in pipes under bending. Eng. Fract. Mech. 77, 415–436.
Cicero, S., Ainsworth, R.A., Gutiérrez-Solana, F., 2010. Engineering approaches for the assessment of low constraint fracture conditions: a critical review. Eng. Fract. Mech. 77, 1360–1374.
Dassault Systèmes, 2007a. ABAQUS Theory Manual. Dassault Systèmes, Providence, RI.
Dassault Systèmes, 2007b. ABAQUS, Ver. 6.7-4. Dassault Systèmes, Providence, RI.
English, S., Arakere, N.K., Allen, P.A., 2010. J–T characterized stress fields of surface cracked metallic liners bonded to a structural backing – I. Uniaxial tension. Eng. Fract. Mech. 77, 170–181.
Evans, A.G., Riley, P.L., 1983. Progress in Nitrogen Ceramics. Martinus Nijhoff Publishers, The Netherlands. 595.
Faleskog, J., 1995. Effects of local constraint along three-dimensional crack fronts – a numerical and experimental investigation. J. Mech. Phys. Solids 43, 447–493.

Gao, X., Zhang, T., Hayden, M., Roe, C., 2009. Effects of the stress state on plasticity and ductile failure of an aluminum 5083 alloy. Int. J. Plasticity 25, 2366–2382.
Gao, X., Zhang, T., Zhuo, J., Graham, S.M., Hayden, M., Roe, C., 2010. On stress-state dependent plasticity modeling: significance of the hydrostatic stress, the third invariant of stress deviator and the non-associated flow rule. Int. J. Plasticity. doi:10.1016/j.ijplas.2010.05.004.
Giner, E., Fernández-Zúñiga, D., Fernández-Sáez, J., Fernández-Canteli, A., 2010. On the J_{x1}-integral and the out-of-plane constraint in a 3D elastic cracked plate loaded in tension. Int. J. Solids Struct. 47, 934–946.
Healy, B., Gullerud, A., Koppenhoefer, K., Roy, A., RoyChowdhury, S., Walters, M., Bichon, B., Cochran, K., Carlyle, A., Dodds, R., 2009. WARP3D-Release 16.2.4, User Manual.
Henry, B.S., Luxmoore, A.R., 1997. The stress triaxiality constraint and the Q-value as a ductile fracture parameter. Eng. Fract. Mech. 57, 375–390.
Huespe, A.E., Needleman, A., Oliver, J., Sánchez, P.J., 2009. A finite thickness band method for ductile fracture analysis. Int. J. Plasticity 25, 2349–2365.
Hutchinson, J.W., 1968a. Plastic stress and strain fields at a crack tip. J. Mech. Phys. Solids 15, 337–347.
Hutchinson, J.W., 1968b. Singular behavior at the end of a tensile crack in a hardening material. J. Mech. Phys. Solids 16, 13–31.
Irwin, G.R., Paris, P.C., 1971. In: Liebowitz, H. (Ed.), Fracture, vol. III. Academic Press, New York.
Iwamoto, T., Tsuta, T., 2002. Computational simulation on deformation behavior of CT specimens of TRIP steel under mode I loading for evaluation of fracture toughness. Int. J. Plasticity 18, 1583–1606.
Kikuchi, M., 1995. A study on three-dimensional crack tip fields. Int. J. Pres. Ves. Pip. 63, 315–326.
Kim, Y., Chao, Y.J., Zhu, X.K., 2003. Effect of specimen size and crack depth on 3D crack-front constraint for SENB specimens. Int. J. Solids Struct. 40, 6267–6284.
Larsson, S.G., Carlsson, A.J., 1973. Influence of non-singular stress terms and specimen geometry on small-scale yielding at crack tips in elastic–plastic materials. J. Mech. Phys. Solids 21, 263–277.
Leach, A.M., Daniewicz, S.R., Newman Jr., J.C., 2007. A new constraint based fracture criterion for surface cracks. Eng. Fract. Mech. 74, 1233–1242.
Li, H., Chandra, N., 2003. Analysis of crack growth and crack-tip plasticity in ductile materials using cohesive zone models. Int. J. Plasticity 19, 849–882.
Li, H., Fu, M.W., Lua, J., Yang, H., 2010. Ductile fracture: experiments and computations. Int. J. Plasticity. doi:10.1016/j.ijplas.2010.04.001.
MacLennan, I., Hancock, J.W., 1995. Constraint-based failure assessment diagrams. Int. J. Pres. Ves. Pip. 64, 287–298.
McClintock, F.A., 1971. In: Liebowitz, H. (Ed.), Fracture, vol. III. Academic Press, New York.
McMeeking, R.M., Parks, D.M., 1979. On criteria for J-dominance of crack-tip fields in large-scale yielding. Elastic-Plastic Fracture, ASTM STP 668, pp. 175–194
Mirone, G., Corallo, D., 2010. A local viewpoint for evaluating the influence of stress triaxiality and lode angle on ductile failure and hardening. Int. J. Plasticity 26, 348–371.
O'Dowd, N.P., 1995. Applications of two parameter approaches in elastic–plastic fracture mechanics. Eng. Fract. Mech. 52, 445–465.
O'Dowd, N.P., Shih, C.F., 1991. Family of crack-tip characterized by a triaxiality parameter – I. Structure of fields. J. Mech. Phys. Solids 39, 989–1015.
O'Dowd, N.P., Shih, C.F., 1992. Family of crack-tip characterized by a triaxiality parameter – II. Fracture applications. J. Mech. Phys. Solids 40, 936–939.
O'Dowd, N.P., Shih, C.F., 1994. Two-parameter fracture mechanics: theory and applications. Fracture Mechanics, vol. 24, ASTM STP 1207, pp. 21–47.
Panayotounakos, D.E., Markakis, M., 1991. Analytical solutions of mixed mode plane strain crack problems in elastic perfectly plastic materials. Int. J. Plasticity 7, 847–863.
Paul, T.K., Khan, A.S., 1998. A centrally cracked thin circular disk, part I: 3D elastic–plastic finite element analysis. Int. J. Plasticity 14, 1209–1239.
Quest Reliability LLC, 2007. FEA-Crack Ver. 3.1.56. Quest Reliability LLC, Berlin.
Rice, J.R., 1974. Limitations to the small scale yielding approximation for crack tip plasticity. J. Mech. Phys. Solids 22, 17–26.
Rice, J.R., Rosengren, G.F., 1968. Plane strain deformation near a crack tip in a power-law hardening material. J. Mech. Phys. Solids 16, 1–12.
Sharma, S.M., Aravas, N., 1991. Determination of higher-order terms in asymptotic elastoplastic crack tip solutions. J. Mech. Phys. Solids 39, 1043–1072.
Sharma, S.M., Aravas N., Zelman, M.G., 1995. Two-parameter characterization of crack tip fields in edged-cracked geometries: plasticity and creep solutions. Fracture Mechanics, ASTM STP, 1220, pp. 309–327.
Shih, C.F., 1973. Elastic–Plastic Analysis of Combined Mode Crack Problems. PhD Thesis. Harvard University.
Shih, C.F., 1974. Small-scale yielding analysis of mixed mode plane-strain crack problems. Fracture Analysis. ASTM STP 560, pp. 187–210.
Shih, C.F., O'Dowd, N.P., Kirk, M.T., 1993. A framework for quantifying crack tip constraint. Constraint Effects in Fracture. ASTM STP 1171. pp. 2–20
Silva, L.A.L., Cravero, S., Ruggieri, C., 2006. Correlation of fracture behavior in high pressure pipelines with axial flaws using constraint designed test specimens. Part II: 3-D effects on constraint. Eng. Fract. Mech. 73, 2123–2138.
Sun, X., Choi, K.S., Liu, W.N., Khaleel, M.A., 2009. Predicting failure modes and ductility of dual phase steels using plastic strain localization. Int. J. Plasticity 25, 1888–1909.
Varias, A.G., Shih, C.F., 1993. Quasi-static crack advance under a range of constraints – steady-state fields based on a characteristic length. J. Mech. Phys. Solids 41, 835–861.
Wang, Y.Y., 1993. On the two-parameter characterization of elastic–plastic crack-front fields in surface-cracked plates. Constraint Effects in Fracture. ASTM STP 1171. pp. 120–138.
Wang, X., 2009. Two-parameter characterization of elastic–plastic crack front fields: surface cracked plates under tensile loading. Eng. Fract. Mech. 76, 958–982.
Wang, Y.Y., Parks, D.M., 1995. Limits of J-T characterization of elastic–plastic crack-tip fields. Constraint Effects in Fracture Theory and Applications, vol. 2. ASTM STP 1244. pp. 43–67.
Wei, Y., Xu, G., 2005. A multiscale model for the ductile fracture of crystalline materials. Int. J. Plasticity 21, 2123–2149.
Williams, M.L., 1957. On the stress distribution at the base of a stationary crack. J. Appl. Mech. 24, 111–114.
Xia, L., Shih, C.F., 1995. Ductile crack growth – II. Void nucleation and geometry effects on macroscopic fracture behavior. J. Mech. Phys. Solids 43, 1953–1981.
Xue, Z., Pontin, M.G., Zok, F.W., Hutchinson, J.W., 2010. Calibration procedures for a computational model of ductile fracture. Eng. Fract. Mech. 77, 492–509.
Yuan, H., Brocks, W., 1991. On the J-integral concept for elastic–plastic crack extension. Nucl. Eng. Des. 131, 157–173.
Zhu, X.K., Chao, Y.J., 2000. Fully plastic crack-tip fields for CCP and DECP specimens under tension in non-hardening materials. Int. J. Solids Struct. 37, 577–598.